Langmuir–Blodgett Films of Amphiphilic Polysilanes Bearing a Pendant Ammonium Moiety

Takahiro Seki*

Research Laboratory of Resources Utilization, Tokyo Institute of Technology, 4259 Nagatsuta, Midori-ku, Yokohama 226, Japan

Nobutaka Tanigaki, Kiyoshi Yase, Akira Kaito, Takashi Tamaki, and Katsuhiko Ueno

National Institute of Materials and Chemical Research, 1-1 Higashi, Tsukuba, Ibaraki 305, Japan

Yuji Tanaka

Daikin Industries Company Ltd., 1-1 Nishi, Hitotsuya, Settu, Osaka 566, Japan

Received November 4, 1994; Revised Manuscript Received May 3, 1995[⊗]

ABSTRACT: Eight homologous amphiphilic polysilanes bearing an ammonium moiety in the side substituent were synthesized. The spreading behavior at the air–water interface of these polysilanes, molecular film fabrication by the Langmuir–Blodgett (LB) technique, and their UV absorption properties and structural features were investigated. The UV absorption spectrum of the transferred LB films was dependent on the deposition condition, such as the existence of a hydrophobic counteranion in the substrate and the magnitude of mechanical compression by the moving barrier. Such spectral changes should be coupled with conformational changes, i.e., *trans*/*gauche* populational changes of the Si backbone modified at the air–water interface. A related conformational modification was achieved when the polysilane monolayer was mixed with stearic acid as the lateral spacer. Polarized UV spectroscopy revealed that the Si backbone is preferentially oriented along the dipping direction possibly due to flow orientation on the water surface. This orientational order depended strongly on the molecular structure of the polysilane and the deposition number. The hydrocarbon side chain, the layer structure, and the morphology of the LB films were evaluated by Fourier transform infrared spectroscopy, transmittance electron microscopy, and X-ray reflectometry. These measurements put forth a view that the LB films are composed of periodical double layers having a homogeneous and amorphous character. Furthermore, a multilayered LB film having the aligned Si backbone promoted homogeneous alignment of a nematic liquid crystal in the dipping direction.

1. Introduction

Polysilanes (polysilylens), Si catenated polymers, have recently received increasing attention because of their intriguing and unusual electrical, photochemical, and optical properties attributed to the delocalized σ-electron in the Si backbone.[1] A great deal of knowledge has been accumulated on polysilanes in the three-dimensional state such as in solutions and in the bulk. Preparation of a monolayer of polysilanes at the air–water interface and application of the Langmuir–Blodgett (LB) technique could allow the study of a bidimensional molecular material and should therefore give a better understanding of the interchain packing and conformational states of these polymers. Such interfacial molecular handling gives structure-controlled films in the nanometer scale, and the molecular films obtained in this manner may have some features that deviate from the properties of the bulk materials. Since the photochemical and electronic properties are strongly coupled with their Si main-chain conformation, the backbone itself acts as a spectroscopic reporter for the structural characterization of the ultrathin molecular films. The LB investigation of ordinary alkyl- and aryl-substituted polysilanes is difficult due to lack of hydrophilicity for interaction with the water surface. Nevertheless, the following research groups have carried out LB studies on chemically functionalized polysilanes.

Embs et al.[2] first reported LB work on polysilanes having bis(butoxyphenyl) substituents that generate stiff backbones to form a rodlike structure. With their polysilanes, the ether linkage was found to be essential for spreading as a monolayer on the water subphase. Due to the stiffness of these materials, highly oriented LB films were generated with their backbone aligned parallel to the dipping direction. Neher et al.[3] described nonlinear optical properties (third-harmonic generation) of these highly oriented LB multilayers.

Hayase's group[4,5] synthesized polysilanes bearing a phenol group in the substituent that are well suited for LB film preparation. Introduction of the phenol moiety was achieved by protection with a trialkylsilyl group during the Wurtz-type condensation polymerization. Some of these polysilanes were found to form highly in-plane oriented LB films, and the orientational order was discussed on the basis of polarized fluorescence data.[5,6] More recently, hydroxyalkyl- and alkoxyalkyl-substituted polysilanes have been exploited,[7] and the anisotropy of the thermochromism with regard to the dipping direction was observed in the LB films of a poly[bis(alkoxyalkyl)silane].

Brynda et al.[8] synthesized poly(methylphenylsilane) bearing π-conjugated electron acceptor substituents and prepared LB films for observation of the electric and photoelectric properties of these substances. Although the polysilanes did not seem to be fully spread as a monolayer on the water surface, the utility of LB deposition for evaluation of the resistivity and photoconductivity at the metal/LB film contact region was demonstrated.

[⊗] Abstract published in *Advance ACS Abstracts,* June 15, 1995.

0024-9297/95/2228-5609$09.00/0

Chart 1

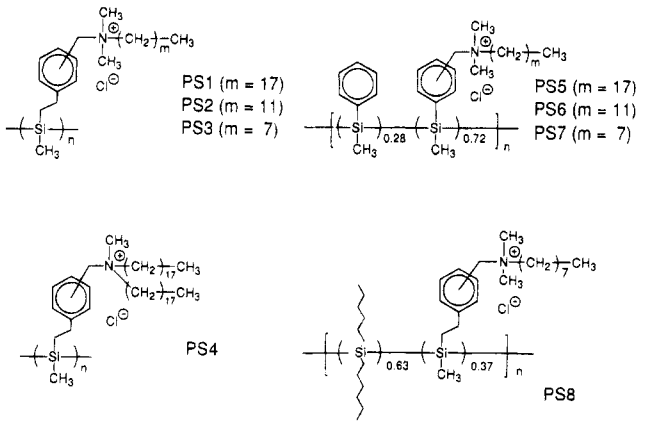

We have focused our efforts on LB investigations using polysilanes which bear ammonium substituents.[9,10] Preliminary experiments[9,10] revealed that the polysilanes with a long alkylammonium moiety form stable monolayers on water and are readily transferred onto a solid substrate by the LB method. Another type of polysilane LB film can be prepared from a water-soluble polysilane that is ion-complexed with an arachidic acid monolayer at the air–water interface.[11] We report herein our expanded investigation, presenting the results of a detailed LB study using the eight ammonium-containing amphiphilic polysilanes indicated in Chart 1 (**PS1**–**PS8**). The other important aim of the present study is to conduct precise structural characterization. Although the orientational information on the Si main chain has formerly been obtained by polarized UV absorption measurements,[9,10] other measurements for structural justification such as X-ray reflectometry, FT-IR spectroscopy, and electron microscopy are required for a detailed understanding of the film structure.

2. Experimental Section

2.1. Materials. The silane monomers methyl(β-phenethyl)dichlorosilane, methylphenyldichlorosilane, and di-*n*-hexyldichlorosilane were purchased from Chisso/Petrarch Systems and distilled before use. All tertiary amines except for *N*-methyldioctadecylamine and chloromethyl methyl ether were purchased from Tokyo Kasei Kogyo Co. and used without purification. Anhydrous tin(IV) chloride was obtained from Wako Pure Chemicals Co.

***N*-Methyldioctadecylamine.** *N*-Methyloctadecylamine (15 g, 0.053 mol), octadecyl bromide (17.7 g, 0.053 mol), and ground sodium carbonate (11.2 g, 0.1 mol) in ethanol (200 mL) were heated at reflux for 70 h. The inorganic salts were filtered off while hot, and the filtrate was evaporated. The residue was dissolved in ether (100 mL) and washed twice with water. After drying over anhydrous $MgSO_4$, the solvent was evaporated. The residual solid was recrystallized twice from acetone: yield 52%, mp 40 °C, in good agreement with that in the literature.[12]

2.2. Preparation of Amphiphilic Polysilanes. The preparation of the ammonium-type amphiphilic polysilanes is shown in Scheme 1. Note that this scheme represents only the essence of the reaction. The starting polysilanes were obtained by the conventional Wurtz-type coupling.[1,13] The phenyl group was chloromethylated and then quaternized with a tertiary trialkylamine in tetrahydrofuran at refluxing temperature. The synthesis was performed under dim red light or in the dark. The structure of the intermediate and final polysilanes was confirmed by ^1H nuclear magnetic resonance (NMR) spectroscopy using a JEOL GSX-270. The molecular weight of the starting and chloromethylated polysilanes was estimated by gel permeation chromatography (polystyrene standard) performed on a Shimadzu LC-5A chromatograph

Scheme 1

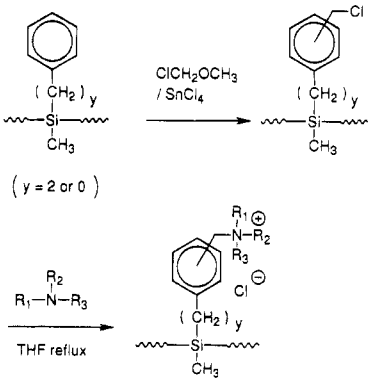

equipped with a Shodex A-805 column. Detailed procedures are given below.

2.2.1. Wurtz-Type Condensation. Sodium condensation for synthesis of the prepolymer was performed essentially according to the procedure of Rabolt et al.[13] Dispersed sodium (0.2 mol) and methyl(β-phenethyl)dichlorosilane or methylphenyldichlorosilane (0.1 mol) were refluxed in toluene/diethylene glycol diethyl ether (diglyme) (80/20 by volume) for 3 h. The reaction mixture was poured into 2-propanol (2 L). The resulting precipitate was dissolved in benzene (300 mL), washed twice with water, and dried over anhydrous $MgSO_4$. This benzene solution was evaporated to a volume of 50 mL, and the polymer was reprecipitated by pouring the solution into 2-propanol. The precipitate was dried under reduced pressure to yield 22% and 37.5% for poly[methyl(β-phenethyl)-silane] (**PS-A**; $M_w = 2.1 \times 10^4$, $M_w/M_n = 1.23$) and poly(methylphenylsilane) (**PS-B**; $M_w = 2.8 \times 10^4$, $M_w/Mn = 1.30$), respectively.

For the copolymer, the precursor of **PS8**, the reaction was performed with a mixture of di-*n*-hexyldichlorosilane (0.05 mol) and methyl(β-phenethyl)dichlorosilane (0.025 mol), giving poly[di-*n*-hexylsilane-*co*-methyl(β-phenethyl)silane] (**PS-C**; $M_w = 1.2 \times 10^5$, $M_w/M_n = 1.8$) in 8.3% yield. The copolymerization ratio was 0.63 (*n*-dihexyl):0.37 (methyl(β-phenethyl)), which was determined on the basis of the relative signal intensity of aromatic protons in the β-phenethyl unit to methyl protons in the *n*-dihexyl unit in the ^1H-NMR analysis.

2.2.2. Chloromethylation. The phenyl group of the starting polysilanes (**PS-A**, **PS-B**, and **PS-C**) was chloromethylated by the same method of Ban et al.[14]

PS-A (2.0 g) was dissolved in 20 mL of chloroform and cooled in an ice bath, and then 20 mL of chloromethyl methyl ether was added. $SnCl_4$ (2 g) was slowly added under nitrogen, and the solution was stirred for 6 h at ice bath temperature and 10 h at room temperature. After adding 50 mL of chloroform, the solution was washed with water twice, dried over anhydrous $MgSO_4$, and evaporated to 10-mL volume. This concentrated polymer solution was poured into methanol (200 mL), and the precipitate obtained was dried under reduced pressure. A white powder of chloromethylated **PS-A** was obtained in 95% yield ($M_w = 2.8 \times 10^4$, $M_w/M_n = 1.30$). In the ^1H-NMR spectrum, the chloromethylene protons showed a broad peak ranging from 4.2 to 4.7 ppm in $CDCl_3$. ^1H-NMR also revealed that the chloromethylation proceeded quantitatively.

The chloromethylation of **PS-B** was performed under relatively mild conditions because, for the aryl-substituted polysilane, the phenyl group is readily replaced by chlorine in the presence of a Lewis acid.[1b] The reaction time for this polymer was 4 h at ice bath temperature. The other procedures were carried out in the same manner as for **PS-A**. A white product was obtained in 97% yield. Due to the short reaction time, the percentage of chloromethylation was 72%.

Chloromethylation of **PS-C** was achieved by a procedure similar to that used for **PS-A**. A completely chloromethylated white powder was obtained in 80% yield.

2.2.3. Quaternization with Tertiary Amines. Chloromethylated polysilanes were successively reacted with tertiary amines in refluxing tetrahydrofuran to provide amphiphilic polysilanes. When the polymer started to precipitate during

Table 1. Quaternization Reaction with Tertiary Amines

target polymer	starting polymer[a]	tertiary amine	reaction condition	yield/%
PS1	**PS-A**	*N,N*-dimethyloctadecylamine	THF,[b] reflux 20 h	76
PS2	**PS-A**	*N,N*-dimethyldodecylamine	THF + ethanol,[c] reflux 6 h	66
PS3	**PS-A**	*N,N*-dimethyloctylamine	THF + ethanol,[c] reflux 12 h	79
PS4	**PS-A**	*N*-methyldioctadecylamine	THF, reflux 120 h	55
PS5	**PS-B**	*N,N*-dimethyloctadecylamine	THF + ethanol,[c] reflux 16 h	59
PS6	**PS-B**	*N,N*-dimethyldodecylamine	THF + ethanol,[c] reflux 12 h	83
PS7	**PS-B**	*N,N*-dimethyloctylamine	THF + ethanol,[c] reflux 6 h	68
PS8	**PS-C**	*N,N*-dimethyloctylamine	THF, reflux 12 h	65

[a] **PS-A**: poly[methyl(β-phenethyl)silane]. **PS-B**: poly(methylphenylsilane). **PS-C**: poly[di-*n*-hexylsilane-*co*-methyl(β-phenethyl)silane]. [b] Tetrahydrofuran. [c] When the polymer started to precipitate during the reaction, a small portion of ethanol was added to the reaction solution.

the reaction, typically within 10–30 min, a small portion of ethanol was added to make a homogeneous solution. Reaction conditions and the results of the quaternization reaction are summarized in Table 1. The final products were purified twice by precipitation from tetrahydrofuran in *n*-hexane. From the ^{1}H-NMR analysis, the quaternization proceeded completely; i.e., the peak due to the chloromethylene protons was completely replaced by ammoniomethylene signals at 4.6–5.6 ppm.

2.3. Methods and Characterization. 2.3.1. LB Film Preparation. The amphiphilic polysilanes were spread under dim red light from freshly prepared chloroform solutions (ca. 1×10^{-3} unit mol dm^{-3}) on a Lauda FW-1 film balance filled with doubly distilled water or an aqueous salt solution (NaCl or $NaClO_4$ at $(5–6) \times 10^{-4}$ mol dm^{-3}). After the solvent evaporated, the monolayer was compressed at the speed of 50 cm^2 min^{-1} and the surface pressure was recorded versus the area per Si unit at 20–21 °C. For the LB deposition, the monolayer was compressed at a given surface pressure and was transferred onto quartz plates (1 × 3 cm; dipping along the longer side) by the vertical dipping technique at a dipping speed of 0.6 cm min^{-1} for both the up and down strokes. The procedure for cleaning the quartz substrates has been described previously.[15] The substrate was finally subjected to an ozone treatment using an ORC UV dry processor VUM-3073-B.

2.3.2. UV Absorption Spectroscopy. UV absorption and dichroism experiments on LB films were carried out on a Jasco HSSP-3 spectrophotometer equipped with a polarizer transparent that is in the region above 215 nm.

2.3.3. Fourier Transform Infrared (FT-IR) Spectroscopy. Transmission FT-IR experiments were performed with a Perkin-Elmer 1800 instrument equipped with a deuterium triglycine sulfate (DTGS) detector at room temperature. Twenty scans at the resolution of 2.0 cm^{-1} were collected and averaged. For the out-of-plane hydrocarbon orientation, an angle-dependent absorption spectrum was measured with a tilting apparatus attachment.

2.3.4. X-ray Reflectometry. X-ray diffractometry was performed with a Rigaku RU-300 at room temperature. The specimens were scanned at 0.2° θ/min in the reflection geometry using Cu Kα radiation monochromatized by a pyrolyzed graphite.

2.3.5. Transmission Electron Microscopy (TEM). Multilayered LB films on a quartz plate were covered with a vacuum-deposited carbon film that was amorphous at the nanometer scale. The reinforced film were stripped off from the substrate in a diluted hydrofluoric acid solution. The floating films were scooped up onto Cu grids. After drying, images were taken by an electron spectroscopic imaging transmission electron microscope (ESI-TEM),[16] a Zeiss CEM-902, at an accelerating voltage of 80 kV.

In the ESI-TEM electrons transmitted through the specimen were selected by a mirror/prism type energy filter and only the electrons scattered either elastically or inelastically by the specimen were imaged. High-contrast pictures were produced by means of the electron spectroscopic imaging mode, which is a method suitable for obtaining fine structures in the films consisting of light elements such as carbon, nitrogen, and oxygen.

2.3.6. Evaluation of LC Alignment.[15] A nematic liquid crystal (DON-103, RODIC, c-17-n-73-i) was sandwiched between two quartz substrates modified by the polysilane LB films in the antiparallel manner (8 μm thickness). The orientation of the liquid crystal in the out-of-plane and in-plane modes was evaluated by observing the absorptivity of an anthraquinone type dichroic dye (LCD-118, Nippon Kayaku Co.) dissolved (1 wt %) in the liquid crystal phase.

3. Results and Discussion

3.1. Spreading Behavior at the Air–Water Interface. 3.1.1. On the Backbone Structure and Salt Addition in the Subphase. Figure 1 presents the surface pressure–area (π–*A*) curves per Si unit at 20 °C for **PS1** (a), **PS5** (b), and **PS8** (c). Solid and dashed lines commonly indicate data on pure water and $NaClO_4$ (6×10^{-4} mol dm^{-1}) solution, respectively. On a $NaClO_4$ aqueous subphase, all polysilanes formed more condensed monolayers than on pure water. Since a NaCl solution at an identical concentration did not cause such contraction (Figure 1a, dotted line), the monolayer contraction at the interface is attributed to the anion exchange from Cl^- to ClO_4^-, a more hydrophobic one. It is thus concluded that the film contraction is attained by the reduced electrostatic repulsion force among the ammonium moieties.

The limiting area per Si unit, extrapolation of the steepest region to zero surface pressure, for **PS1** (0.45–0.57 nm^2) and **PS5** (0.45–0.6 nm^2) was much larger for the cross section of a vertically oriented long alkyl chain (0.2 nm^2), suggesting that the molecular dimension of the condensed surface monolayers is determined by the bulky part around the Si unit.

For the copolymer-type amphiphile **PS8**, on the other hand, the apparent limiting area per Si unit was small (0.17–0.22 nm^2). Supposedly, the spread layer should contain folded structures protruding toward the air in the hydrophobic dihexylsilane unit part of the Si main chain due to lack of hydrophilicity of this unit. We observed that **PS8** exhibits a partial thermochromic behavior originated from poly(di-*n*-hexylsilane) in methanol.[17] Therefore, the copolymer seems to contain block-type segments in the main chain rather than those in a statistically random state. Wurtz-type sodium condensation of two dichlorosilane monomers, in general, has been found to give a blocky backbone of the two components as confirmed by ^{29}Si-NMR analysis.[18–20] In this context, the spread film of **PS8** on the water surface should be viewed as a highly folded film, and the picture of the Si chain array running fairly parallel to the water surface seems to be improbable.

3.1.2. On the Side-Chain Structure. Figure 2 displays π–*A* isotherms on a $NaClO_4$ aqueous solution at 20 °C, for methyl(β-phenethyl)silane-based series (**PS1–PS4**, a) and methylphenylsilane-based series (**PS5–PS7**, b). All of the polysilanes examined here having an alkyl chain of more than an eight-carbon

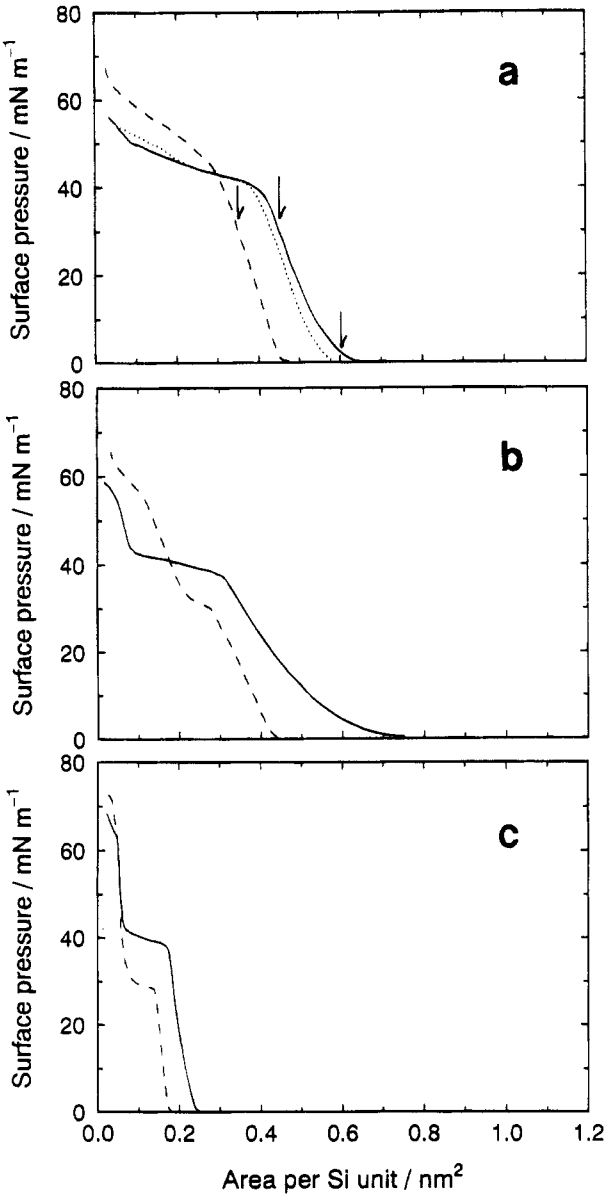

Figure 1. Surface pressure–area isotherms per Si unit of **PS1** (a), **PS5** (b), and **PS8** (c) on pure water (solid curve), NaCl (dotted curve), and $NaClO_4$ (dashed curve) aqueous solutions at the concentration of 6×10^{-4} mol dm^{-3} at 20 °C. The arrows refer to the transfer conditions for UV spectroscopic measurements shown in Figure 4.

length were insoluble in water and formed stable monolayers. When a trimethylammonium group (one carbon length) was introduced in the side chain, the polymer was readily soluble in water and the monolayer formation was impossible. It is already reported that LB film preparation of this water-soluble polymer is possible when the polymer is ion-complexed with a monolayer of an amphiphile anion at the air–water interface.[11]

For the single alkyl chain polymers (**PS1**–**PS3** and **PS5**–**PS7**), the lift-off area of the surface pressure on a $NaClO_4$ subphase was almost identical, around 0.45 nm^2. An increase in the chain length from C_8 to C_{18} influenced, although not significantly, stability against compression. If the compression property of the monolayers is compared at a constant area, for instance, 0.3 nm^2, the monolayer having the longer carbon length endures the larger surface pressure.

The double-chain polymer **PS4** gave a somewhat larger lift-off area (>0.5 nm^2; Figure 2a), possibly due

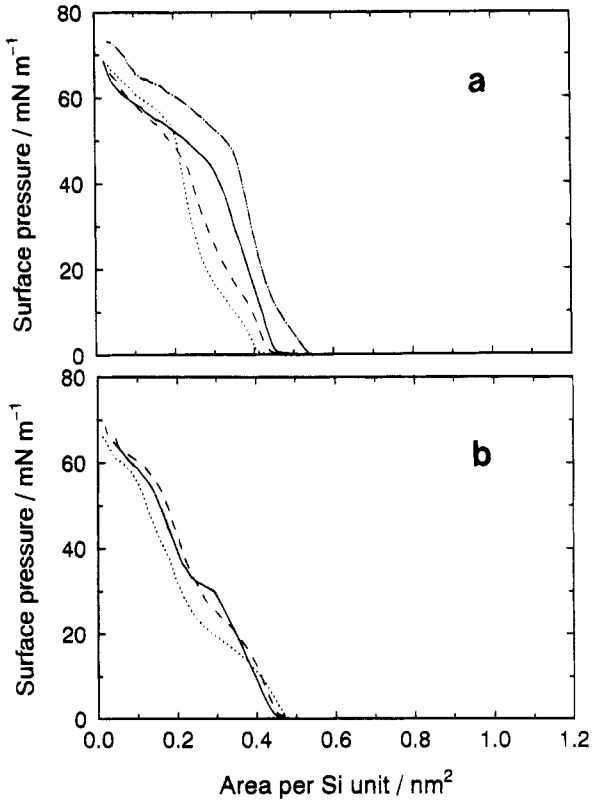

Figure 2. Surface pressure–area isotherms per Si unit on a $NaClO_4$ aqueous solution (5×10^{-4} mol dm^{-3}) at 20 °C for the series of methyl(β-phenethyl)silane-based amphiphilic polymers (a) and the series of methylphenylsilane-based amphiphilic polymers (b). The upper part (a) contains curves of **PS1** (—), **PS2** (– –), **PS3** (···), and **PS4** (– · –), and the lower part (b) contains those of **PS5** (—), **PS6** (– –), and **PS7** (···).

to the lateral steric requirement. However, this area increase was less than expected for addition of a long alkyl chain, further implying that the monolayer dimension is mainly determined by the bulky part around the silane unit and that the alkyl side chains of the monolayer are in the air phase and loosely packed.

3.1.3. Monolayers Mixed with Stearic Acid. The alkyl side chains in the monolayer do not seem to be packed closely. This observation inspired us to prepare mixed monolayers of **PS1** with another long-chain component. Since the polysilanes under investigation are cationic, an anionic amphiphile was expected to be effectively incorporated into the monolayers. For this reason, stearic acid (**SA**) was chosen as the mixing material. The mixing ratio **PS1** (1)/**SA** (x) was changed from x of 1 to 4 on the $NaClO_4$ aqueous subphase (Figure 3). Adding **SA** led to an expansion of the area per Si unit of the polymer, but the low concentrations of **SA** ($x = 1$ and 2) caused less expansion, suggesting that a molecular mixing of **PS1** and **SA** occurs at low concentrations. In contrast, further addition of **SA** ($x = 3$ and 4) caused regular expansion by ca. 0.2 nm^2 with x, indicating that at the latter stage **SA** spreads independently and a phase-separated monolayer is seemingly formed.

It is noteworthy that the shape of the π–A curve and the lift-off area of the **PS1** (1)/**SA** (1) monolayer (dashed curve in Figure 4) resembled that of **PS4** (Figure 2a), which suggests a similarity in the monolayer structure. Actually, both amphiphilic polysilanes bear two C_{18} chains per Si unit. The difference between the two monolayers, **PS1** (1)/**SA** (1) and **PS4**, is solely the linkage mode; i.e., the former has one covalent-bonded

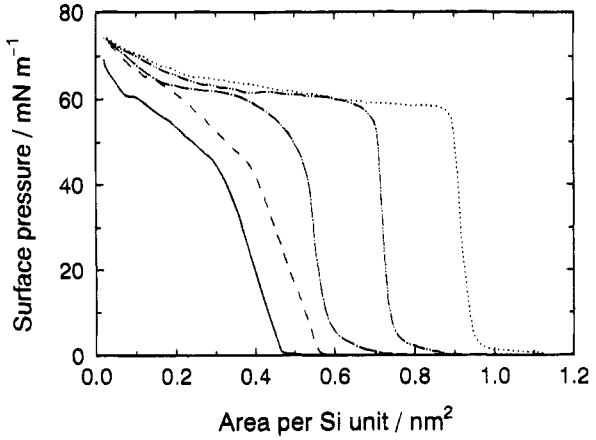

Figure 3. Surface pressure–area isotherms per Si unit on a $NaClO_4$ aqueous solution (5×10^{-4} mol dm^{-3}) at 20 °C of binary mixed monolayers of **PS1** with stearic acid (**SA**). The mixing molar ratio of **SA** to **PS1** (x) is 0 (—), 1 (– –), 2 (– · –), 3 (– · · –), and 4 (· · ·).

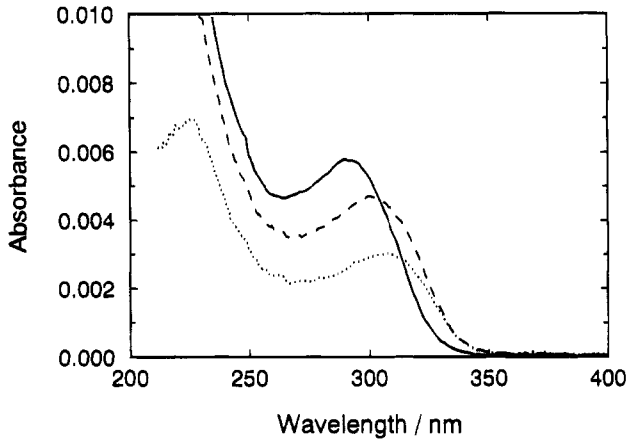

Figure 4. UV absorption spectra of transferred monolayers of **PS1** on both sides of a quartz substrate. Transfer conditions are indicated by arrows in Figure 1a. The area per Si unit is 0.60 (· · ·), 0.45 (– –), and 0.35 nm^2 (—).

and one ion-complexed C_{18} chains and the latter has two covalently bonded double C_{18} chains.

3.2. UV Absorption of Transferred LB Films. 3.2.1. Effect of the Monolayer Area. The monolayers were readily transferred as a single LB layer from all subphases examined, but multilayers were successfully obtained only from a $NaClO_4$ aqueous subphase in the Y mode.

For the polysilane **PS1**, the surface pressures selected for one-layer transfer were 2 and 30 mN m^{-1} on pure water and 30 mN m^{-1} on a $NaClO_4$ aqueous solution. These three transfer conditions are indicated by the three arrows in Figure 4. They correspond to the area per Si unit of 0.60, 0.45, and 0.35 nm^2, respectively. The σ–σ^* absorption band around 300 nm exhibited a clear continuous blue shift as the monolayer area was reduced. The magnitude of shift was approximately 20 nm. The spectral shift should be attributed to conformational changes of the σ-conjugated Si backbone from an expanded state to a more condensed state, namely, enhancement of the *gauche* conformer in the Si backbone. The motive force of the continuous conformational changes should be the requirement of the area limitation that the monolayer occupies in a two-dimensional interface, and the spectral shift can be regarded as an example of the piezochromic effect. Song et al.[21] reported the piezochromic behavior of solvent-cast solid

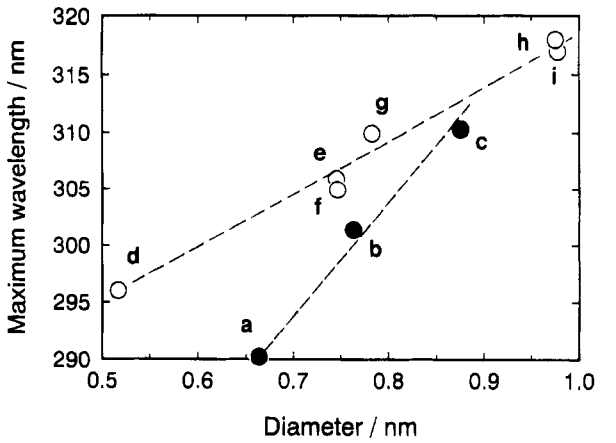

Figure 5. Relationship between the peak maximum of the first σ–σ^* band and the supposed diameter occupied by the Si unit. The diameter for the present monolayer (closed circles) was calculated simply assuming a circle of the corresponding area indicated in Figure 1. Symbols a–c correspond to the areas of 0.35, 0.45, and 0.60 nm^2, respectively. Data in solutions (open circles) are taken from the paper of Harrah and Zeigler:[22] The substituents of polysilanes are [methyl, methyl] (d), [*n*-hexyl, methyl] (e), [β-phenethyl, methyl] (f), [*n*-dodecyl, methyl] (g), [*n*-hexyl, *n*-hexyl] (h), and [cyclohexyl, methyl] (i).

films of polysilanes. In these solid films, the static pressure induces both red and blue shifts in the absorption spectrum, depending on the structure of the organic substituents and the magnitude of the pressure applied. Since the Si backbone of **PS1** is supposed to lie parallel to the water surface, the pressure applied by the moving barrier of the LB trough should induce axial compression rather than lateral compression and the resulting distortion is manifested by the blue shift. Our earlier report[10] pointed out that the spectral shift is present at the air–water interface before the LB transfer, which implies that conformational modification does not occur at the meniscus region during the transfer.

Harrah and Zeigler[22] demonstrated that the wavelength of the Si band absorption maximum in solution is dependent on the dimension of the two alkyl substituents attached to the Si atom; less bulky substituents lead to a more blue-shifted spectrum. They suggest that the shift stems from steric interference of the substituents which results in straining the Si backbone and/or backbone conformational preference. Their observation and interpretation agrees with ours in that the wavelength of the σ–σ^* band is a function of the given space (in solution) or area (in monolayer) per Si unit (Figure 5).

PS5 was also transferred at various areas in the same manner as for **PS1**, and the spectroscopic properties were examined. The spectral change for this material was much less sensitive to area variation. A blue shift of only a few nanometers around 330 nm was observed upon compression. This insensitivity may arise from more restricted rotation about the Si–Si bond to which the bulky aromatic group is directly attached.

3.2.2. In-Plane Orientation of the Si Chain. The transition moment of the first σ–σ^* band around 300 nm is parallel to the Si chain direction.[23] Therefore, the Si chain orientation is readily estimated by polarized UV absorption spectroscopy. Figure 6 displays polarized UV absorption spectra of (a) 9-layered **PS1** and (b) 21-layered **PS8** deposited from the surface of a $NaClO_4$ solution at 25 mN m^{-1}. The electric vector of the polarized light in normal incidence was set parallel

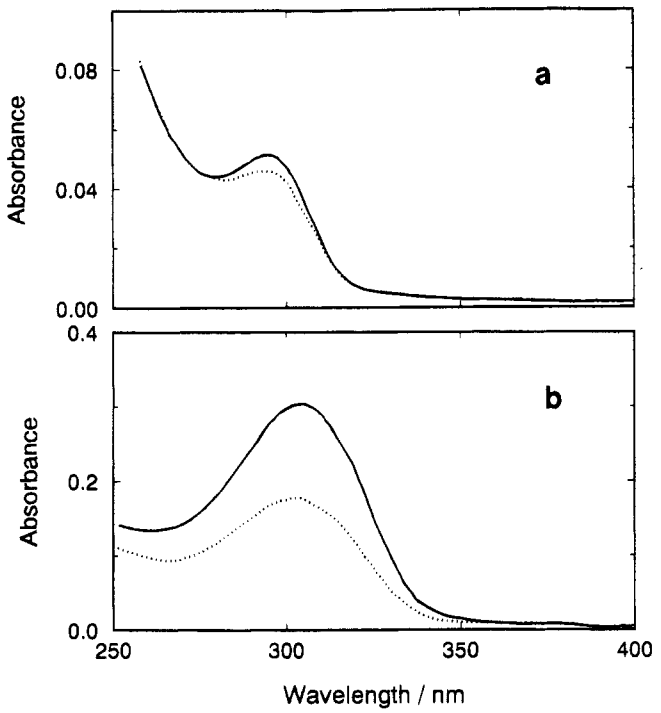

Figure 6. Polarized UV absorption spectra of LB films of 9-layered **PS1** (a) and 21-layered **PS8** (b) on both sides of a quartz plate. Absorption spectra were taken in normal incidence with the linearly polarized light set parallel (solid line) and orthogonal (dotted line) to the dipping direction.

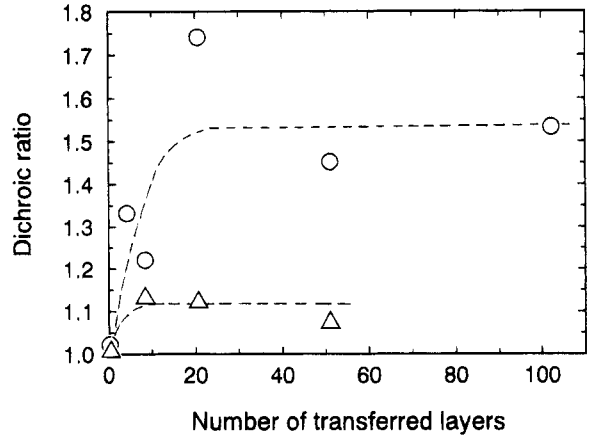

Figure 7. Dichroic ratios of the LB films due to the backbone orientation along the dipping direction as a function of the number of transferred layers. Triangles and circles are data for **PS1** and **PS8**, respectively.

(solid curve) and perpendicular (dotted curve) to the dipping direction. The absorptivity of the $\sigma-\sigma^*$ band for both samples was larger when the polarization plane was parallel to the dipping direction, indicating that the polymer backbone preferentially aligns parallel to the dipping direction.

Figure 7 presents the dichroic ratio of the LB films as a function of the number of transferred layers. In both materials, the in-plane dichroic ratio enhanced with the increased number of depositions up to ca. 20 layers and then saturated. From the dependence on the deposition number, the Si main chain is seemingly aligned by the flow orientation on the water surface as a consequence of the successive deposition processes rather than the force field at the meniscus on the substrate.[24] Agreement of the UV spectra of the monolayer on the water subphase and those transferred onto the solid substrate (see section 3.2.1) further supports this interpretation.

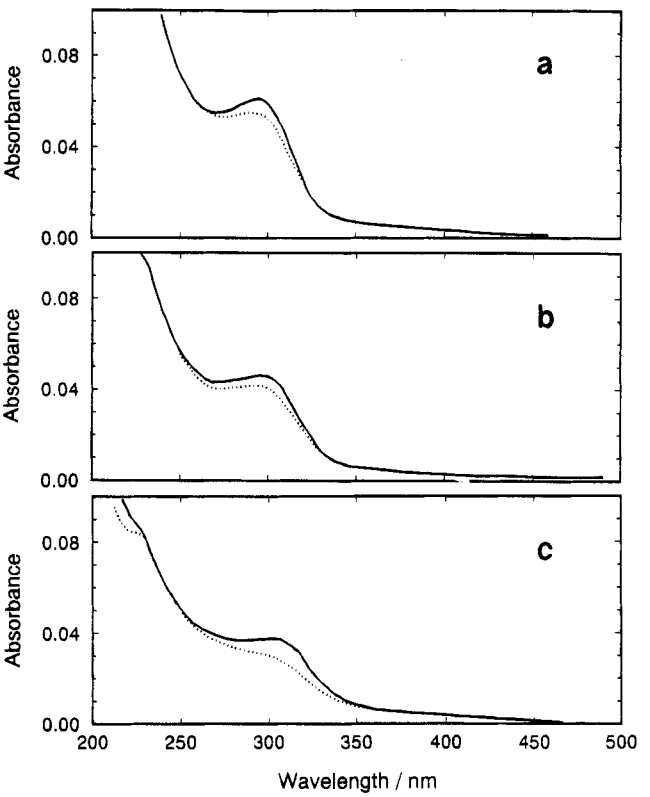

Figure 8. Polarized UV absorption spectra of LB films of nine-layered **PS1** mixed with **SA**. Monolayers were transferred at 25 mN m^{-1} on both sides of a quartz substrate from the surface of a $NaClO_4$ aqueous subphase. The molar mixing ratios of **SA** to **PS1**, (x) are 0 (a), 1 (b), and 4 (c). Solid and dotted lines are the same for those indicated in Figure 6.

The dichroic ratio obtained with **PS1** is rather small (ca. 1.1); however, it is improved with **PS8** (>1.5 for the sufficiently large deposition number). Some of the other polysilane LB films reported by both Embs et al.[2] and Kani et al.[5,7] are highly oriented in the dipping direction. Such LB films have a dichroic ratio of more than 3. We assume that high flexibility and lack of stereoregularity for our polysilanes are responsible for the rather poor orientation. Introduction of the di-*n*-hexylsilane component in **PS8** improved the orientational order, but we are not able, at the moment, to present a plausible explanation for this. It seems difficult to deduce definitive orienting factors from the molecular structure alone. In fact, Kani et al.[5] have demonstrated that a very subtle change in the substituent structure of their materials influences the orientational order in a crucial manner.

3.2.3. Mixed Monolayers of PS1 and SA. As suggested in section 1.3, one or two **SA** molecules can be effectively incorporated into the **PS1** monolayer. Thus, molecular mixing of **SA** may change the conformational state and stiffness of the spread **PS1** monolayer. Figure 8 displays the changes in the UV absorption spectra of nine-layered LB films of **PS1** mixed with **SA** at a mixing ratio x of 0, 1, and 4. An increase in the **SA** content induced a slight red shift of the $\sigma-\sigma^*$ band peaked from 290 ($x = 0$) to 302 nm ($x = 4$). This implies an expansion of the Si chain brought about by insertion of the long chain of the **SA** molecule as the laterial spacer. For the monolayer of $x = 4$, the dichroic ratio was meaningfully enhanced to 1.3 (Figure 8c) from 1.1 obtained for $x = 0$ and 1 (Figure 8a,b).

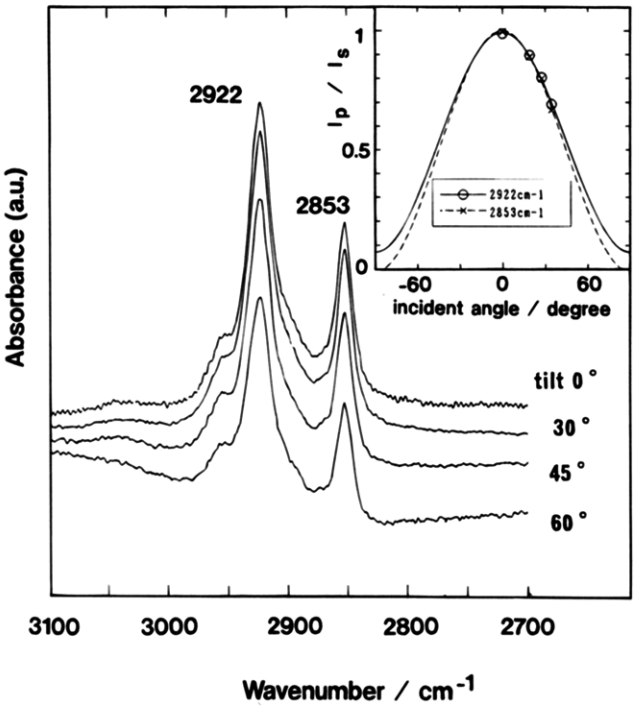

Figure 9. FT-IR spectra in the region of CH_2 stretching bands of 43-layered **PS1**. Out-of-plane tilt angles of the specimen are indicated in the spectra. The inset presents the relative band intensity observed at the four tilt angles. In the ordinate, the band intensity observed with p-polarized light (I_p) is divided by that with s-polarized light (I_s) for correction of observing area changes resulting from the tilt arrangement. Note that the deviation of the tilt angle in the inset figure from those shown in the spectrum stems from the correction using refractive indices of the polysilane and glass.

3.3. FT-IR Spectroscopy. UV absorption measurements provide information only on the Si backbone. Structural information about the hydrocarbon side chain of the polymer can be obtained by FT-IR spectroscopy. Transmission FT-IR spectra of CH_2 stretching bands of a 43-layered LB film on a glass slide (Matsunami glass) of **PS1** are indicated in Figure 9.

The intense bands at 2853 and 2922 cm^{-1} are assigned to the CH_2 symmetric and antisymmetric stretching modes of the *n*-octadecyl hydrocarbon chain. It is known that the frequencies of CH_2 stretching bands are sensitive to the conformation of the hydrocarbon chain;[25,26] low frequencies (2920 and 2850 cm^{-1}) of the bands are characteristic of the highly ordered (*trans zigzag*) alkyl chain, while their shifts to higher frequencies are indicative of the increase in conformational disorder containing *gauche* conformers.[25] Judging from the position of the observed CH_2 symmetric band, 2853 cm^{-1}, the hydrocarbon chain in the **PS1** LB film is not ordered but should contain considerable amounts of *gauche* conformers. The frequency value of this LB film is comparable to that of hydrocarbon chains in a lipid bilayer membrane in the fluid liquid crystalline state above the thermal phase transition temperature.[25]

With regard to the out-of-plane orientation, measurements were made varying the tilt angles ranging from 0 to 60° from the surface normal. The larger tilt angle gave the smaller absorbance, indicating that the hydrocarbon side chain orients statistically perpendicular to the substrate plane. The inset of the figure depicts the relative absorption intensity against the tilt angle corrected for the refractive index of the polysilane. The solid and dashed lines indicate cosine curves fitted to the four experimental points assuming the ideal normal orientation of the hydrocarbon chain.

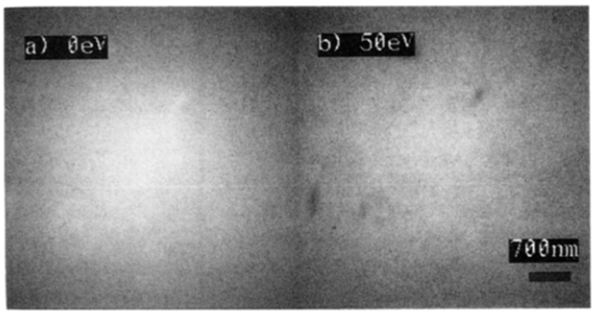

Figure 10. TEM images of the **PS8** film recorded by using (a) zero loss and (b) 50-eV loss electrons.

Measurements of polarized transmission FT-IR were undertaken to evaluate the in-plane anisotropy of the hydrocarbon chain. Practically no difference, however, in the absorptivity of the CH_2 stretching band was observed for the measurements at various in-plane angles. Thus, it is found that the in-plane orientation of the Si main chain as proved by the polarized UV absorption measurements (section 3.2.2) is not reflected in the orientation of the side hydrocarbon chain.

3.4. TEM Observation. TEM images were taken for LB films of **PS1** and **PS8**. The two LB films gave essentially the same images. A typical TEM image is shown in Figure 10 for 21-layered **PS8**. In the zero-loss image (a), there is no fine structure except for thick molecular coagulations with a size of submicrometers. The similar structure having opposite contrast can be seen in the energy loss image (b). This means that white dots in a and black ones in b should be molecular assembly introduced during deposition or handling. The electron diffraction from the area of 100 nm to 10 μm revealed only the halo. It was found that the LB films have no structure in the films' plane.

3.5. X-ray Reflection. The structure of the LB layers of **PS1** and **PS8** was investigated by small-angle X-ray scattering in reflection geometry. The X-ray reflection profile of both films exhibited two characteristic features, a periodical modulation of the reflectivity, the so-called Kiessig fringes, and one Bragg peak. A typical profile is shown in Figure 11 for **PS1** and **PS8**. The Kiessig fringes give the overall thickness of the films, and the Bragg peak provides the long spacing (d) of the layer structure. In this study, these parameters were calculated by simply applying Bragg's law. The structural data obtained by these experiments are summarized in Table 2. The X-ray reflections at the wide-angle range were also taken. However, no obvious structure except for the higher order reflection from the layer spacing was observed in the profile, indicating that no appreciable crystalline structure exists within the LB films. Thus, the LB films are regarded as comprised of amorphous and homogeneous layers.

The layer spacing, d, should correspond to that of the double layer length because the LB films are constantly transferred in the Y mode and the number of Keissig fringes was half of the deposition number. The layer spacing, d, is too large for a single layer structure and should indicate the length of the bilayer. Postulating the side chain of **PS1** to be expanded as *trans* zigzag conformers, the length from the silicon atom to the terminal methyl group of the hydrocarbon chain is ca. 7 nm for a double layer. On the other hand, the length measured from the ammonium nitrogen to the terminal methyl group, as a double layer, is ca. 5 nm. Consider-

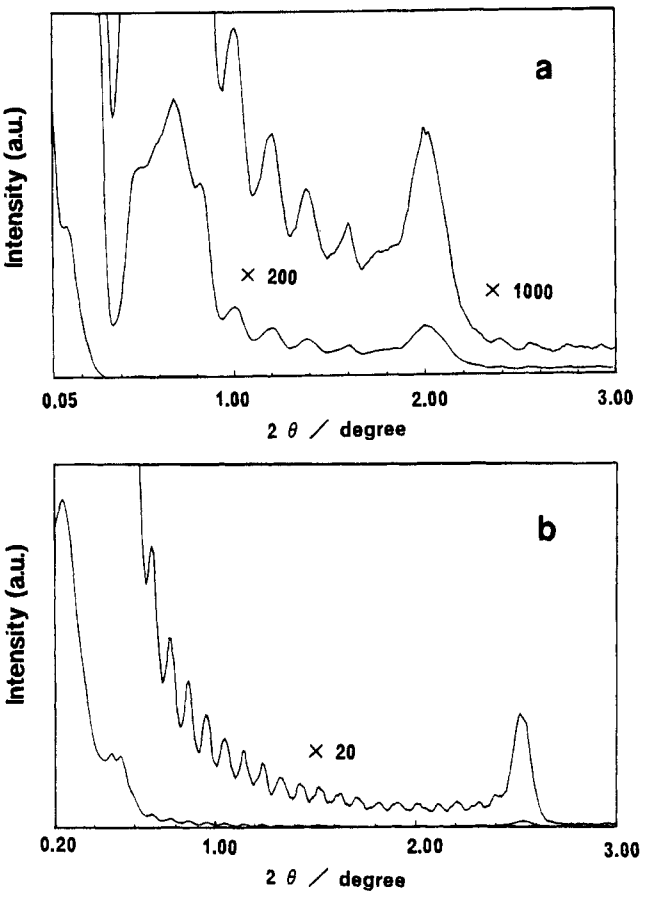

Figure 11. Small-angle X-ray reflection from a 21-layered **PS1** LB film (a) and a 51-layered **PS8** LB film (b).

Table 2. Layer Structure Evaluated by X-ray Reflectivity

polysilane	no. of transferred layers	layer spacing[a] (d)/nm	film thickness[b]/nm
PS1	21	4.42	51.1
	43	4.31	90.4
PS8	51	3.50	92.0

[a] Determined by a Bragg peak. [b] Determined by Kiessig fringes. Note that the layer spacing corresponds to the length of a double layer; therefore, the film thickness is half of the multiplication of the layer spacing by the number of transferred layers.

ing a fairly perpendicular orientation of the side hydrocarbon chain to the substrate plane without tilting as indicated by the FT-IR experiments (section 3.3), the observed value, d = 4.3–4.4 nm, is in reasonable agreement with the latter length (5 nm). The lower length could result from involvement of considerable amounts of *gauche* conformers. Thus, we present a picture in which the ammonium moieties are positioned at the interface of the double layers and the Si main chain is located at the middle. A plausible illustration for the double-layered structure of the **PS1** LB film is drawn in Figure 12.

The long spacing of **PS9**, d = 3.5 nm, is approximately 20% smaller than that of **PS1**, possibly due to the shorter length of the alkyl side chain. We would not expect a quantitative agreement for the layer length because there exists ambiguity in the main-chain structure which is possibly composed of blocky segments (see section 3.1.1).

3.6. Alignment of a Nematic Liquid Crystal. Evaluation of liquid crystal alignment on LB films has been recognized as a powerful technique to understand

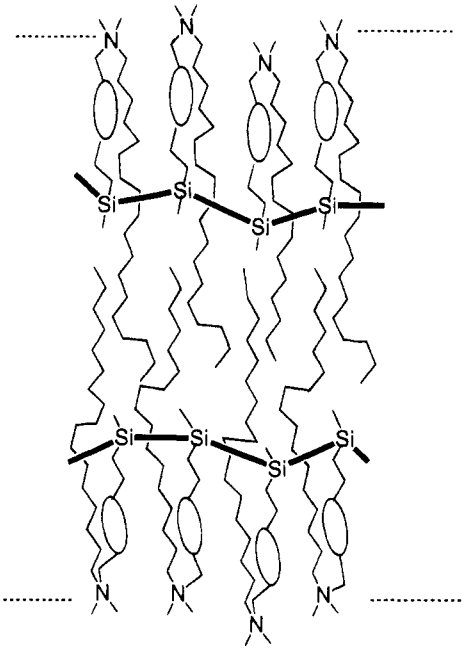

Figure 12. Schematic illustration of a plausible double-layered structure of **PS1** in the multilayered LB film.

Chart 2

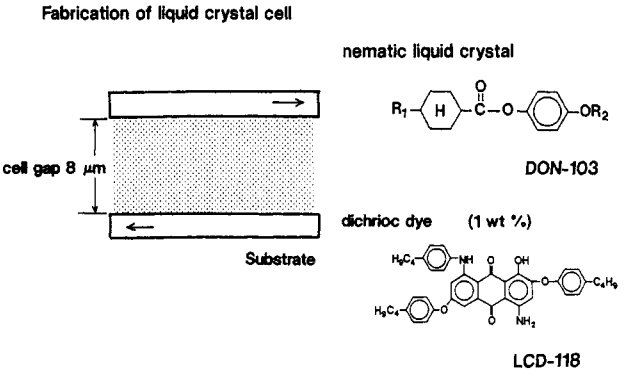

the surface nature of various kinds of molecular films.[5,15,27-30] Alignment of liquid crystals is particularly sensitive to molecular orientation, surface energy, topology, and the homogeneity of the surface layer. It is, therefore, of value to study liquid crystal alignment as a means of characterizing the surface of the LB films.

It is generally recognized that the packing state and orientation of molecules in a single monolayer is different from that in a built-up multilayer even though identical LB materials are used. Therefore, the alignment behavior of these two cases was examined. Alignment of a nematic liquid crystal, DON-103, was evaluated by observing the system through the crossed polarizers. For the studies of in-plane orientation, a dichroic dye, LCD-118, was added and the angular dependence of the light absorption was observed through a polarized film. The two substrates were set in an antiparallel manner (Chart 2). The results are summarized in Table 3. **PS1** and **PS2** having linear C_{18} and C_{12} alkyl chains gave only homeotropic (perpendicular to the substrate plane) alignment at any deposition numbers. This is in agreement with the description in the Cognard's monograph[31] that fatty amines and alkyl-substituted ammonium derivatives having chains with a carbon content over 10 promote homeotropic alignment. On the other hand, **PS3** and **PS8** with side-chain carbon numbers of less than 8 promoted planar

Table 3. Alignment of a Nematic Liquid Crystal on Polysilane LB Films

polysilane	single monolayer	built-up monolayers (no. of layers)
PS1	⊥[a]	⊥ (21)
PS2	⊥	⊥ (9)
PS3	r[b]	r (9)
PS8	r	//[c] (21)

[a] Homeotropic. [b] Planar but not homogeneous. [c] Homogeneous, with the liquid crystal orientation being parallel to the dipping direction.

or tilted alignment. A noteworthy result is found for the multilayered **PS8** (21 layers). This polysilane LB surface gave homogeneous alignment in which the liquid crystal orientation was parallel to the dipping direction. The in-plane orientation was not controlled for **PS3** and single-layered **PS8**.

These data may be correlated with the in-plane orientational order presented in Figures 6 and 7. Figure 6a is the dichroic spectra of **PS1**, but that of **PS3** having an identical Si backbone gave almost an equal orientational order. It is hence assumed that the homogeneous alignment imposed by the dipping process requires some good degree of orientational order in the Si main chain provided that the side alkyl chain is not too long. The possibility that the liquid crystal is aligned by surface topological factors such as macroscopic grooved structures can be ruled out from the fact that the X-ray reflectivity exhibits clear Kiessig fringes (see section 3.5) which is indicative of surface smoothness, and TEM observation gives clear evidence for the flatness of the surface (see Figure 10). Thus, it is concluded that the aligning ability of the nematic liquid crystal originates from backbone orientation rather than surface topology. It is to be noted that Kani et al.[5] already reported that homogeneous alignment of a nematic liquid crystal, 4-cyano-4′-*n*-pentylbiphenyl (5CB) is attained on a highly oriented polysilane LB film. Their polysilane possesses a short (n-butyl) alkyl chain and a *m*-phenol group as the substituents.

4. Conclusion

Polysilanes have been recognized as fascinating materials exhibiting unique optical and electrical functions. We find that application of the LB technique for this material is able to modulate conformations and orientation which cannot be attained by a simple casting method. Also it provides quite homogeneous and defined layer-structured polysilane ultrathin films. These materials may be of interest in the fields of microelectronics and microoptics. Our present materials suffer from an ambiguity in the primary chemical structure, i.e., lack of stereoregularity in the primary chemical structure, i.e., lack of stereoregularity on the Si atom and uncontrolled substitution position of the introduced ammonium moiety on the phenyl ring. Our future work will include preparation of well-defined polysilane molecules because primary structure would be connected directly to the assembled structure and resulting electronic and optical properties.

References and Notes

(1) For reviews, see: (a) Miller, R. D.; Michl, J. *Chem. Rev.* **1989**, *89*, 1359. (b) West, R. *J. Organomet. Chem.* **1988**, *300*, 327. See also references cited therein.
(2) Embs, F. W.; Wegner, G.; Neher, D.; Albouy, P.; Miller, R. D.; Willson, C. G.; Schrepp, W. *Macromolecules* **1991**, *24*, 5068.
(3) Mittler-Neher, S.; Neher, D.; Stegeman, G. I.; Embs, F. W.; Wegner, G. *Chem. Phys.* **1992**, *161*, 289.
(4) Nakano, Y.; Murai, S.; Kani, R.; Hayase, S. *J. Polym. Sci., Part A: Polym. Chem.* **1993**, *31*, 3361.
(5) Kani, R.; Yoshida, H.; Nakano, Y.; Murai, S.; Mori, Y.; Kawata, Y.; Hayase, S. *Langmuir* **1993**, *9*, 3045.
(6) Yoshida, H.; Kani, R.; Hayase, S.; Horie, K. *J. Phys. Chem.* **1993**, *97*, 5370.
(7) Kani, R.; Nakano, Y.; Majima, Y.; Hayase, S.; Yuan, C.-H.; West, R. *Macromolecules* **1994**, *27*, 1911.
(8) Brynda, E.; Koropecky, I.; Kminek, I.; Nespurek, S.; Schnabel, W. *Polym. Adv. Technol.* **1994**, *5*, 257.
(9) Seki, T.; Tamaki, T.; Ueno, K. *Macromolecules* **1992**, *25*, 3825.
(10) Seki, T.; Tamaki, T.; Ueno, K.; Tanaka, Y. *Thin Solid Films* **1994**, *243*, 625.
(11) Seki, T.; Tohnai, A.; Tamaki, T.; Ueno, K. *J. Chem. Soc., Chem. Commun.* **1993**, 1876.
(12) Staudinger, H.; Rössler, K. *Ber. Dtsch. Chem. Ges.* **1936**, *69*, 49.
(13) Rabolt, J. H.; Hofer, D.; Miller, R. D.; Fickes, G. N. *Macromolecules* **1986**, *19*, 611.
(14) Ban, H.; Sukegawa, D.; Tagawa, A. *Macromolecules* **1987**, *20*, 1775.
(15) Seki, T.; Sakuragi, M.; Kawanishi, Y.; Suzuki, Y.; Tamaki, T.; Fukuda, R.; Ichimura, K. *Langmuir* **1993**, *9*, 211.
(16) Reimer, L.; Fromm, I.; Hulk, C.; Rennekamp, A. *Microsc. Microanal. Microstr.* **1992**, *3*, 141.
(17) Seki, T.; Tanaka, Y.; Tamaki, T., unpublished results.
(18) Wolff, A. R.; Nozue, I.; Maxka, J.; West, R. *J. Polym. Sci., Part A: Polym. Chem.* **1988**, *26*, 701.
(19) Sakamoto, K.; Yoshida, M.; Sakurai, H. *Macromolecules* **1990**, *23*, 4494.
(20) Schilling, F. C.; Lovinger, A. C.; Davis, D. D.; Bovey, F.; Zeigler, J. M. *Macromolecules* **1992**, *25*, 2854.
(21) (a) Song, K.; Miller, R. D.; Wallraff, G. M.; Rabolt, J. F. *Macromolecules* **1991**, *24*, 4084. (b) Song, K.; Miller, R. D.; Wallraff, G. M.; Rabolt, J. F. *Macromolecules* **1992**, *25*, 3629.
(22) Harrah, L. A.; Zeigler, J. M. *Macromolecules* **1987**, *20*, 601.
(23) Tachibana, H.; Kawabata, Y.; Koshihara, S.; Arima, T.; Moritomo, Y.; Tokura, Y. *Phys. Rev. B* **1991**, *44*, 5487.
(24) Schwiek, S.; Vahlenkamp, T.; Xu, Y.; Wegner, G. *Macromolecules* **1992**, *25*, 2513.
(25) Sapper, H.; Cameron, D. G.; Mantsch, H. H. *Can. J. Chem.* **1981**, *59*, 2543.
(26) Katayama, N.; Ozaki, Y.; Seki, T.; Tamaki, T.; Iriyama, K. *Langmuir* **1994**, *10*, 1898.
(27) Hiltrop, K.; Hasse, J.; Stegemeyer, H. *Ber. Bunsen-Ges. Phys. Chem.* **1994**, *98*, 209.
(28) Mino, N.; Nakajima, K.; Ogawa, K. *Langmuir* **1991**, *7*, 1468.
(29) Zhu, Y.-M.; Lu, Z.-H.; Wei, Y. *Jpn. J. Appl. Phys.* **1993**, *32*, L1462.
(30) Suzuki, M.; Ferencz, A.; Iida, S.; Enkelmann, V.; Wegner, G. *Adv. Mater.* **1993**, *5*, 359.
(31) Cognard, J. *Mol. Cryst. Liq. Cryst., Suppl. Ser. 1* **1982**, 21.

MA9463122